Effect of High Pressure on the Crystal Structures of Polymorphs of l-Histidine

SUPPLEMENTARY MATERIAL

The Effect of High Pressure on the Crystal Structures of Polymorphs of *L*-Histidine

Giulia Novelli,[1] Helen E. Maynard-Casely,[2] Garry J. McIntyre,[2] Mark R. Warren[3] and Simon Parsons[*1]

1. Centre for Science at Extreme Conditions and EaStCHEM School of Chemistry, The University of Edinburgh, King's Buildings, West Mains Road, Edinburgh, Scotland, EH9 3FD, UK.

2. Australian Nuclear Science and Technology Organisation, New Illawarra Road, Lucas Heights, NSW 2234, Australia.

3. Diamond Light Source, Harwell Campus, Oxfordshire, OX11 0DE, UK

Electronic Supplementary Information Table of Contents

Table S1 Phase behaviour of polymorphs at high pressure from the Cambridge Structural Database (v 5.41, Nov 2019) and literature.

	Ambient Pressure			High pressure		
	Form	**Space group**	**Refcode / Temperature**	**Form**	**Space group**	**Phase behavior**
***P*-aminobenoic acid**	α	*P* 2_1/n	AMBNAC06 / 293 K[1]	δ	*P* n	δ-form can be recovered at ambient conditions. Direct compression of the α-form at ~0.85 GPa (water). Solution recrystallization: AMBNAC14 / 0.49 GPa (ethanol) AMBNAC15 / 0.33 GPa (water) AMBNAC18 / 0.8 GPa (water and ethanol)[2,3]
	β	*P* 2_1/n	AMBNAC04 / 298 K[5]			α-form and β-form are phase stable up to ~13 GPa (Raman spectroscopy).[4]
	γ	*P* na2_1	AMBNAC09 / 100 K[6]			
Chloropropamide	α	*P* $2_12_12_1$	BEDMIG10 / 295 K[7]	α'	*P* $2_1$11	BEDMIG18 / 3.33 GPa[8] The same phase transition is observed for a dry powder sample of the α-form at 5.5 GPa.[9]
	β	*P* bcn	BEDMIG01 / 295 K[10]			β-form undergoes different phase transitions depending on the choice of pressure-transmitting medium (Ne, He, paraffin, 1:1 pentane-isopentane).[11,12]
	ε	*P* na2_1	BEDMIG04 / 295 K[14]			β-form and ε-form transform to different phases depending on the type of mechanical treatment.[13]
	δ	*P* bca	BEDMIG03 / 295 K[14]			
	γ	*P* 2_1	BEDMIG19 / 293 K[11]			
Piracetam	I	*P* 2_1/n	BISMEV03 / 293 K[15]			
	II	*P* $\bar{1}$	BISMEV / 293 K[17]	V	*P* $\bar{1}$	BISMEV10 / 4.0 GPa[18] Forms I, II and III interconversion under mechanical activation and pressing.[16]
	III	*P* 2_1/n	BISMEV13 / 290 K[19]	IV	*P* 21/n	BISMEV04 / 0.4 GPa[20]
Tolazamide	I	*P* $\bar{1}$	CABCUD03 / 295 K[21]			Forms I and II are stable up to 6.1 GPa and 6.8 GPa, respectively (pentane-isopentane pressure transmitting medium). Incomplete I-II transition in methanol at 0.1 GPa. Tolazamide-I and II have similar bulk moduli, 6.4(3) and 5.8(2) GPa respectively.[22]
	II	*P* $\bar{1}$	CABCUD35 / 295 K[23]			
Glycine	α	*P* 21/n	GLYCIN20 / 301 K[24]			α-Form is phase stable up to 6.2 (GLYCIN64),[25] 6.4 GPa (neutron powder diffraction),[26] 50 GPa (angle-dispersive X-ray diffraction).[27]
	β	*P* 2_1	GLYCIN71 / 293 K[28]	δ	*P* 2_1	GLYCIN62 / 7.8 GPa[28]
	γ	*P* 3_1	GLYCIN18 / 293 K[29]	ε	*P* n	GLYCIN68 / 4.3 GPa[25]
				ζ	*I* 1	DOLBIR43 / 0.0 Gpa[30]

	Ambient Pressure			High pressure		
	Form	Space group	Refcode / Temperature	Form	Space group	Phase behavior
Paracetamol	I	*P* 2_1/n	HXACAN35 / 293 K[31]			Form-I-to-form-II transformation observed in a pressure-cycled powder sample above 4 GPa, not detected when a single-crystal was used. Potentially, *'the monoclinic polymorph is slightly more compressible'* [32]
	II	*P* bca	HXACAN33 / 293 K[35]			Further evidence of the form-I-to-II transition in a later Raman study, which also described additional polymorphs at 8 GPa (form IV) and 10.5 GPa (form V).[33]
	III	*P* $ca2_1$	HXACAN40 / 293 K[36]			Recovery of form II assisted by anti-solvent addition at high pressure.[34]
***L*-cysteine**	I	*P* $2_12_12_1$	LCYSTN36 / 295 K[37]	III	*P* $2_12_12_1$	LCYSTN25 / 4.2 GPa[38] Phase transitions observed by Raman spectroscopy at 2.1 GPa and 2.3 GPa.[39,40]
				IV	*P* 2_1	LCYSTN26 / 1.7 GPa[38]
	II	*P* 2_1	LCYSTN / 293 K[41]			Reversible phase transitions at ~2.9 GPa and ~3.6 GPa observed by Raman spectroscopy.[40]
CL-20	β	*P* $b2_1a$	PUBMUU01 / 293 K[42]			
	γ	*P* 2_1/n	PUBMUU06 / 293 K[42]	ξ	*P* 2_1/n	PUBMUU23 / 3.3 GPa[43]
	ε	*P* 2_1/n	PUBMUU18 / 295 K[44]			Spectroscopic experiments observed a ε-form-to-γ-form transition between 4.1 and 6.4 GPa, which subsequently transforms to the ξ-form at ~18.7 GPa.[45]
ROY	ON	*P* 2_1/c	QAXMEH / 293 K[46]			
	R	*P* $\bar{1}$	QAXMEH02 / 293 K[46]			
	YN	*P* $\bar{1}$	QAXMEH04 / 293 K[46]			
	ORP	*P* bca	QAXMEH05 / 293 K[46]			
	YT04	*P* 2_1/n	QAXMEH12 / 296 K[47]			
	R05	*P* 2_1	QAXMEH31 / 250 K[48]			
	PO13	*P* 2_1/c	QAXMEH52 / 293 K[49]			
	Y	*P* 2_1/n	QAXMEH01 / 293 K[46]			Y-form is phase stable up to 5.2 GPa (QAXMEH21), bulk modulus of 6.0(7).[50]
	OP	*P* 2_1/n	QAXMEH03 / 293 K[46]			OP-form is phase sable up to 9.3 GPa, bulk modulus of 4.3(3).[51]
Benzocaine	I	*P* 2_1/c	QQQAXG04 / 300 K[52]	IV	*P* 2_1/c	QQQAXG15 / 0.78 GPa[53]
	II	*P* $2_12_12_1$	QQQAXG07 / 300 K[54]			

The research in the CSD was performed by selecting structurally characterised organic molecules (R factor < 10) whose ambient-pressure polymorphs have been investigated at high-pressure for comparison, with the highest-pressure structure reported. When available, supplementary studies performed with different techniques were added for completeness.

Table S2 Crystallographic information for all structures. Several crystals were used for each study to confirm reproducibility and 'fill in' large pressure increments.

CCDC Deposition Number	**2020565**	**2020566**	**2020567**	**2020568**	**2020569**
Phase, Pressure (GPa), Crystal #	**I, 0.00**	**I, 0.23, 1**	**I, 0.58, 1**	**I, 1.32, 1**	**I, 1.33, 2**
Crystal data					
Crystal system, space group	Orthorhombic, $P2_12_12_1$	Orthorhombic, $P2_12_12_1$	Orthorhombic, $P2_12_12_1$	Orthorhombic, $P2_12_12_1$	Orthorhombic, $P2_12_12_1$
Temperature (K)	298	293	293	293	293
a, b, c (Å)	5.1586(5), 7.3367(6), 18.7825(13)	5.1558(7), 7.3090(8), 18.817(18)	5.1208(6), 7.1807(7), 18.765(17)	5.0563(4), 6.9875(5), 18.674(12)	5.0631(5), 6.9866(7), 18.655(11)
α, β, γ (°)	90, 90, 90	90, 90, 90	90, 90, 90	90, 90, 90	90, 90, 90
V (Å^3), ρ (g/cm^3)	710.86 (10), 1.450	709.1 (7), 1.453	690.0 (6), 1.494	659.8 (4), 1.562	659.9 (4), 1.562
Radiation type	Mo $K\alpha$, λ = 0.71073 Å	Synchrotron, λ = 0.4859 Å	Synchrotron, λ = 0.4859 Å	Synchrotron, λ = 0.4859 Å	Synchrotron, λ = 0.4859 Å
μ (mm^{-1})	0.11	0.05	0.12	0.06	0.06
Crystal size (mm)	0.35 × 0.30 × 0.15	0.25 × 0.15 × 0.15*	0.25 × 0.15 × 0.15*	0.25 × 0.15 × 0.15*	0.25 × 0.25 × 0.15**
Data collection					
Diffractometer	Agilent SuperNova	Beamline I19-EH2	Beamline I19-EH2	Beamline I19-EH2	Beamline I19-EH2
Absorption correction	Multi-scan	Multi-scan	Multi-scan	Multi-scan	Multi-scan
T_{min}, T_{max}	0.6816, 0.7454	0.6423, 0.7439	0.6688, 0.7439	0.6530, 0.7442	0.6609, 0.7442
No. of measured, independent and observed [$I > 2\sigma(I)$] reflections	8266, 1440, 1251	924, 388, 348	804, 357, 319	925, 442, 365	1609, 657, 535
R_{int}	0.045	0.013	0.011	0.012	0.031
θ_{max}, θ_{max}(°), completeness	2.981, 25.242, 100%	2.044, 15.686, 40%	1.9330, 15.6163, 37%	2.128, 17.726, 34%	2.128, 17.697, 49%
(sin $\theta/\lambda)_{max}$ (Å^{-1})	0.626	0.556	0.554	0.627	0.626
Refinement					
$R[F^2 > 2\sigma(F^2)]$, $wR(F^2)$, S	0.042, 0.069, 1.61	0.059, 0.119, 2.31	0.063, 0.127, 2.46	0.066, 0.144, 2.58	0.039, 0.083, 1.29
No. unique reflections/parameters	1440 / 102	388 / 46	357 / 46	442 / 46	657 / 101
No. of restraints	0	25	25	25	100
$\Delta\rho_{max}$, $\Delta\rho_{min}$ (e Å^{-3})	0.20, -0.16	0.22, -0.18	0.27, -0.21	0.30, -0.25	0.16, -0.19

CCDC Deposition Number	**2020570**	**2020571**	**2020572**	**2020573**	**2020574**
Phase, Pressure (GPa), Crystal #	**I, 2.01, 1**	**I, 2.06, 2**	**I, 2.53, 1**	**I, 3.06, 2**	**I, 3.20, 1**
Crystal data					
Crystal system, space group	Orthorhombic, $P2_12_12_1$	Orthorhombic, $P2_12_12_1$	Orthorhombic, $P2_12_12_1$	Orthorhombic, $P2_12_12_1$	Orthorhombic, $P2_12_12_1$
Temperature (K)	293	293	293	293	293
a, b, c (Å)	5.0093(5), 6.8705(6), 18.569(14)	5.0023(6), 6.8485(8), 18.580(12)	4.9780(5), 6.8013(7), 18.521(15)	4.9447(4), 6.7345(6), 18.434(9)	4.9403(5), 6.7284(7), 18.432(17)
α, β, γ (°)	90, 90, 90	90, 90, 90	90, 90, 90	90, 90, 90	90, 90, 90
V (Å^3), ρ (g/cm^3)	639.1 (5), 1.613	636.5 (4), 1.619	627.1 (5), 1.644	613.9 (3), 1.679	612.7 (6), 1.682
Radiation type	Synchrotron, λ = 0.4859 Å	Synchrotron, λ = 0.4859 Å	Synchrotron, λ = 0.4859 Å	Synchrotron, λ = 0.4859 Å	Synchrotron, λ = 0.4859 Å
μ (mm^{-1})	0.06	0.06	0.06	0.06	0.06
Crystal size (mm)	0.25 × 0.15 × 0.15	0.25 × 0.25 × 0.15	0.25 × 0.15 × 0.15	0.25 × 0.25 × 0.15	0.25 × 0.15 × 0.15
Data collection					
Diffractometer	Beamline I19-EH2	Beamline I19-EH2	Beamline I19-EH2	Beamline I19-EH2	Beamline I19-EH2
Absorption correction	Multi-scan	Multi-scan	Multi-scan	Multi-scan	Multi-scan
T_{min}, T_{max}	0.6591, 0.7442	0.6575, 0.7442	0.6211, 0.7442	0.6727, 0.7442	0.6271, 0.7442
No. of measured, independent and observed [$I > 2\sigma(I)$] reflections	1021, 477, 387	1143, 550, 489	1000, 484, 393	993, 500, 451	924, 453, 348
R_{int}	0.023	0.013	0.030	0.014	0.029
θ_{max}, θ_{max}(°), completeness	2.161, 17.736, 37%	2.167, 17.654, 43%	2.897, 17.704, 38%	2.201, 17.685, 42%	2.918, 17.701, 37%
(sin $\theta/\lambda)_{max}$ (Å^{-1})	0.627	0.624	0.626	0.625	0.626
Refinement					
$R[F^2 > 2\sigma(F^2)]$, $wR(F^2)$, S	0.059, 0.122, 1.90	0.034, 0.076, 1.56	0.064, 0.126, 1.70	0.037, 0.077, 1.60	0.055, 0.106, 1.46
No. unique reflections/parameters	477 / 46	550 / 101	484 / 46	500 / 101	453 / 46
No. of restraints	25	100	25	100	25
$\Delta\rho_{max}$, $\Delta\rho_{min}$ (e Å^{-3})	0.22, -0.21	0.13, -0.16	0.28, -0.26	0.14, -0.15	0.19, -0.22

CCDC Deposition Number	**2020575**	**2020576**	**2020577**	**2020578**	**2020579**
Phase, Pressure (GPa), Crystal #	**I, 3.85, 1**	**I, 4.45, 1**	**I', 4.62, 2**	**I', 5.02, 1**	**I', 5.61, 2**
Crystal data					
Crystal system, space group	Orthorhombic, $P2_12_12_1$	Orthorhombic, $P2_12_12_1$	Orthorhombic, $P2_12_12_1$	Orthorhombic, $P2_12_12_1$	Orthorhombic, $P2_12_12_1$
Temperature (K)	293	293	293	293	293
a, b, c (Å)	4.9065(5), 6.6743(7), 18.352(15)	4.8797(5), 6.6367(7), 18.251(16)	4.8515(5), 6.8861(8), 17.238(11)	4.8335(3), 6.8544(5), 17.230(12)	4.8301(5), 6.8383(10), 17.128(14)
α, β, γ (°)	90, 90, 90	90, 90, 90	90, 90, 90	90, 90, 90	90, 90, 90
V (Å^3), ρ (g/cm^3)	601.0 (5), 1.715	591.1 (5), 1.744	575.9 (4), 1.790	570.8 (4), 1.805	565.7 (5), 1.822
Radiation type	Synchrotron, λ = 0.4859 Å	Synchrotron, λ= 0.4859 Å	Synchrotron, λ = 0.4859 Å	Synchrotron, λ = 0.4859 Å	Synchrotron, λ = 0.4859 Å
μ (mm^{-1})	0.06	0.07	0.07	0.07	0.07
Crystal size (mm)	0.25 × 0.15 × 0.15	0.25 × 0.15 × 0.15	0.25 × 0.25 × 0.15	0.25 × 0.15 × 0.15	0.25 × 0.25 × 0.15
Data collection					
Diffractometer	Beamline I19-EH2	Beamline I19-EH2	Beamline I19-EH2	Beamline I19-EH2	Beamline I19-EH2
Absorption correction	Multi-scan	Multi-scan	Multi-scan	Multi-scan	Multi-scan
T_{min}, T_{max}	0.5481, 0.7442	0.6412, 0.7442	0.6056, 0.7442	0.6306, 0.7442	0.6457, 0.7442
No. of measured, independent and observed [$I > 2\sigma(I)$] reflections	1443, 514, 402	1149, 448, 368	1092, 530, 428	1078, 422, 351	924, 438, 372
R_{int}	0.037	0.024	0.036	0.027	0.022
θ_{max}, θ_{max}(°), completeness	2.220, 17.721, 43%	2.232, 17.723, 38%	2.588, 17.694, 46%	2.186, 17.730, 37%	2.606, 17.712, 41%
(sin $\theta/\lambda)_{max}$ (Å^{-1})	0.626	0.626	0.626	0.627	0.626
Refinement					
$R[F^2 > 2\sigma(F^2)]$, $wR(F^2)$, S	0.050, 0.104, 1.51	0.054, 0.108, 1.79	0.047, 0.097, 1.36	0.048, 0.096, 1.59	0.040, 0.077, 1.43
No. unique reflections/parameters	514 / 46	448 / 46	530 / 101	422 / 46	438 / 101
No. of restraints	25	25	100	25	100
$\Delta\rho_{max}$, $\Delta\rho_{min}$ (e Å^{-3})	0.24, -0.21	0.28, -0.23	0.19, -0.21	0.26, -0.17	0.14, -0.17

CCDC Deposition Number	**2020580**	**2020581**	**2020582**	**2020583**	**2020584**
Phase, Pressure (GPa), Crystal #	**I', 5.86, 1**	**I', 6.60, 1**	**II, 0.00**	**II, 0.11, 1, 1**	**II, 0.44, 1**
Crystal data					
Crystal system, space group	Orthorhombic, $P2_12_12_1$	Orthorhombic, $P2_12_12_1$	Monoclinic, $P2_1$	Monoclinic, $P2_1$	Monoclinic, $P2_1$
Temperature (K)	293	293	298	293	293
a, *b*, *c* (Å)	4.8112(4), 6.8129(5), 17.100(12)	4.7918(3), 6.7777(5), 17.040(11)	5.1698(4), 7.3884(6), 9.4715(7)	5.1632(6), 7.3711(6), 9.466(9)	5.1218(6), 7.2236(5), 9.427(8)
α, β, γ (°)	90, 90, 90	90, 90, 90	90, 98.177 (5), 90	90, 98.082 (19), 90	90, 98.171 (19), 90
V (Å^3), ρ (g/cm^3)	560.5 (4), 1.839	553.4 (4), 1.862	358.10 (5), 1.439	356.7 (3), 1.445	345.2 (3), 1.493
Radiation type	Synchrotron, λ= 0.4859 Å	Synchrotron, λ = 0.4859 Å	Mo $K\alpha$, λ = 0.71073 Å	Synchrotron, λ = 0.4859 Å	Synchrotron, λ = 0.4859 Å
μ (mm^{-1})	0.07	0.07	0.11	0.05	0.06
Crystal size (mm)	0.25 × 0.15 × 0.15	0.25 × 0.15 × 0.15	0.20 × 0.20 × 0.15	0.20 × 0.20 × 0.15	0.20 × 0.20 × 0.15
Data collection					
Diffractometer	Beamline I19-EH2	Beamline I19-EH2	Agilent SuperNova	Beamline I19-EH2	Beamline I19-EH2
Absorption correction	Multi-scan	Multi-scan	Multi-scan	Multi-scan	Multi-scan
T_{min}, T_{max}	0.6639, 0.7442	0.6290, 0.7442	0.5953, 0.7454	0.634, 0.7439	0.6109, 0.7440
No. of measured, independent and observed [$I > 2\sigma(I)$] reflections	1830, 519, 460	728, 395, 325	3651, 1456, 1202	703, 367, 281	838, 404, 299
R_{int}	0.047	0.025	0.035	0.028	0.037
θ_{max}, θ_{max}(°), completeness	2.200, 17.717, 47%	3.653, 17.731, 36%	3.511, 26.378, 100%	2.914, 15.731, 36%	3.511, 16.270, 37%
(sin $\theta/\lambda)_{max}$ (Å^{-1})	0.626	0.627	0.625	0.558	0.577
Refinement					
$R[F^2 > 2\sigma(F^2)]$, $wR(F^2)$, *S*	0.046, 0.099, 1.61	0.047, 0.099, 1.37	0.039, 0.067, 1.26	0.066, 0.125, 1.86	0.064, 0.122, 1.68
No. unique reflections/parameters	519 / 46	395 / 46	1456 / 101	367 / 46	404 / 46
No. of restraints	25	25	0	25	25
$\Delta\rho_{max}$, $\Delta\rho_{min}$ (e Å^{-3})	0.20, -0.21	0.19, -0.18	0.20, -0.18	0.21, -0.20	0.22, -0.19

CCDC Deposition Number	**2020585**	**2020586**	**2020587**	**2020588**	**2020589**
Phase, Pressure (GPa), Crystal #	**II, 0.70, 2**	**II, 0.82, 1**	**II, 0.97, 3**	**II, 1.47, 1**	**II, 1.87, 2**
Crystal data					
Crystal system, space group	Monoclinic, $P2_1$	Monoclinic, $P2_1$	Monoclinic, $P2_1$	Monoclinic, $P2_1$	Monoclinic, $P2_1$
Temperature (K)					
a, b, c (Å)	5.104(3), 7.1487(8), 9.4237(17)	5.0851(6), 7.1064(6), 9.395(8)	5.0767(6), 7.0869(7), 9.402(2)	5.0325(6), 6.9670(6), 9.357(8)	5.006(3), 6.8962(7), 9.3401(19)
α, β, γ (°)	90, 98.23 (4), 90	90, 98.30 (2), 90	90, 98.428 (12), 90	90, 98.73 (2), 90	90, 99.27 (4), 90
V (Å^3), ρ (g/cm^3)	340.3 (2), 1.514	336.0 (3), 1.534	334.62 (9), 1.540	324.3 (3), 1.589	318.3 (2), 1.619
Radiation type	Synchrotron, λ = 0.4859 Å	Synchrotron, λ = 0.4859 Å	Ag $K\alpha$, λ = 0.56086 Å	Synchrotron, λ = 0.4859 Å	Synchrotron, λ = 0.4859 Å
μ (mm^{-1})	0.06	0.06	0.07	0.06	0.06
Crystal size (mm)	0.25 × 0.20 × 0.10	0.20 × 0.20 × 0.15	0.25 × 0.20 × 0.15	0.20 × 0.20 × 0.15	0.25 × 0.20 × 0.10
Data collection					
Diffractometer	Beamline I19-EH2	Beamline I19-EH2	Bruker D8 Venture	Beamline I19-EH2	Beamline I19-EH2
Absorption correction	Multi-scan	Multi-scan	Multi-scan	Multi-scan	Multi-scan
T_{min}, T_{max}	0.6501, 0.7441	0.5434, 0.7440	0.6996, 0.7449	0.5903, 0.7440	0.6538, 0.7442
No. of measured, independent and observed [$I > 2\sigma(I)$] reflections	1374, 565, 496	864, 420, 319	3768, 769, 621	946, 401, 293	713, 423, 390
R_{int}	0.030	0.041	0.034	0.038	0.010
θ_{max}, θ_{max}(°), completeness	2.454, 17.600, 43%	2.951, 16.493, 38%	3.201, 23.587, 42%	2.971, 15.890, 42%	2.522, 17.741, 34%
(sin $\theta/\lambda)_{max}$ (Å^{-1})	0.622	0.584	0.713	0.563	0.627
Refinement					
$R[F^2 > 2\sigma(F^2)]$, $wR(F^2)$, S	0.040, 0.087, 1.41	0.068, 0.132, 1.71	0.054, 0.114, 2.03	0.061, 0.128, 1.92	0.037, 0.082, 1.81
No. unique reflections/parameters	565 / 101	420 / 46	769 / 46	401 / 46	423 / 101
No. of restraints	100	25	25	25	100
$\Delta\rho_{max}$, $\Delta\rho_{min}$ (e Å^{-3})	0.16, -0.17	0.21, -0.20	0.28, -0.21	0.21, -0.24	0.15, -0.15

CCDC Deposition Number	**2020590**	**2020591**	**2020592**	**2020593**	**2020594**
Phase, Pressure (GPa), Crystal #	**II, 2.77, 2**	**II, 3.00, 3**	**II', 3.21, 3**	**II', 3.71, 2**	**II', 4.28, 1**
Crystal data					
Crystal system, space group	Monoclinic, $P2_1$	Monoclinic, $P2_1$	Monoclinic, $P2_1$	Monoclinic, $P2_1$	Monoclinic, $P2_1$
Temperature (K)	293	293	293	293	293
a, b, c (Å)	4.949(3), 6.8093(9), 9.2876(18)	4.9324(10), 6.7931(13), 9.245(4)	4.8807(8), 6.7916(11), 9.192(3)	4.833(3), 6.8184(12), 9.177(2)	4.8215(5), 6.8188(7), 9.163(8)
α, β, γ (°)	90, 100.88 (4), 90	90, 100.81 (3), 90	90, 103.38 (2), 90	90, 104.63 (4), 90	90, 105.17 (2), 90
V (Å^3), ρ (g/cm^3)	307.35 (19), 1.677	304.28 (16), 1.694	296.44 (13), 1.738	292.6 (2), 1.761	290.7 (2), 1.772
Radiation type	Synchrotron, λ = 0.4859 Å	Ag $K\alpha$, λ = 0.56086 Å	Ag $K\alpha$, λ = 0.56086 Å	Synchrotron, λ = 0.4859 Å	Synchrotron, λ = 0.4859 Å
μ (mm^{-1})	0.06	0.08	0.08	0.07	0.07
Crystal size (mm)	0.25 × 0.20 × 0.10	0.25 × 0.20 × 0.15	0.25 × 0.20 × 0.15	0.25 × 0.20 × 0.10	0.20 × 0.20 × 0.15
Data collection					
Diffractometer	Beamline I19-EH2	Bruker D8 Venture	Bruker D8 Venture	Beamline I19-EH2	Beamline I19-EH2
Absorption correction	Multi-scan	Multi-scan	Multi-scan	Multi-scan	Multi-scan
T_{min}, T_{max}	0.6620, 0.7442	0.5972, 0.7445	0.4939, 0.7445	0.6554, 0.7442	0.6053, 0.7442
No. of measured, independent and observed [$I > 2\sigma(I)$] reflections	1042, 493, 437	1421, 464, 340	1346, 410, 343	878, 451, 399	723, 386, 302
R_{int}	0.022	0.065	0.043	0.019	0.025
θ_{max}, θ_{max}(°), completeness	2.552, 17.738, 40%	3.318, 20.548, 38%	3.386, 20.537, 35%	2.575, 17.748, 39%	2.995, 17.752, 34%
(sin $\theta/\lambda)_{max}$ (Å^{-1})	0.627	0.626	0.625	0.627	0.627
Refinement					
$R[F^2 > 2\sigma(F^2)]$, $wR(F^2)$, S	0.058, 0.124, 2.02	0.036, 0.069, 1.04	0.046, 0.098, 1.65	0.052, 0.119, 2.03	0.095, 0.193, 2.96
No. unique reflections/parameters	493 / 46	464 / 101	410 / 101	451 / 46	386 / 46
No. of restraints	25	100	100	25	25
$\Delta\rho_{max}$, $\Delta\rho_{min}$ (e Å^{-3})	0.30, -0.26	0.14, -0.13	0.21, -0.18	0.24, -0.22	0.48, -0.38

CCDC Deposition Number	**2020595**	**2020596**	**2020597**	**2020598**
Phase, Pressure (GPa), Crystal #	**II', 4.62, 2**	**II', 4.98, 1**	**II', 5.20, 3**	**II', 6.85, 1**
Crystal data				
Crystal system, space group	Monoclinic, $P2_1$	Monoclinic, $P2_1$	Monoclinic, $P2_1$	Monoclinic, $P2_1$
Temperature (K)	293	293	293	293
a, b, c (Å)	4.8149(14), 6.8108(6), 9.132(3)	4.7892(5), 6.7998(7), 9.085(8)	4.8007(19), 6.781(2), 9.110(6)	4.7210(8), 6.7249(10), 9.029(14)
α, β, γ (°)	90, 105.37 (2), 90	90, 104.78 (3), 90	90, 105.55 (4), 90	90, 106.16 (4), 90
V (Å^3), ρ (g/cm^3)	288.76 (13), 1.785	286.1 (3), 1.801	285.7 (2), 1.804	275.3 (4), 1.872
Radiation type	Synchrotron, λ = 0.4859 Å	Synchrotron, λ = 0.4859 Å	Ag $K\alpha$, λ = 0.56086 Å	Synchrotron, λ = 0.4859 Å
μ (mm^{-1})	0.07	0.07	0.09	0.07
Crystal size (mm)	0.25 × 0.20 × 0.10	0.20 × 0.20 × 0.15	0.25 × 0.20 × 0.15	0.20 × 0.20 × 0.15
Data collection				
Diffractometer	Beamline I19-EH2	Beamline I19-EH2	Bruker D8 Venture	Beamline I19-EH2
Absorption correction	Multi-scan	Multi-scan	Multi-scan	Multi-scan
T_{min}, T_{max}	0.6524, 0.7442	0.5520, 0.7442	0.6544, 0.7340	0.5850, 0.7442
No. of measured, independent and observed [$I > 2\sigma(I)$] reflections	1124, 458, 390	408, 280, 217	1305, 373, 303	756, 382, 292
R_{int}	0.048	0.018	0.059	0.029
θ_{max}, θ_{max}(°), completeness	2.585, 17.695, 40%	3.021, 17.737, 25%	3.468, 20.541, 34%	3.044, 17.764, 34%
(sin $\theta/\lambda)_{max}$ (Å^{-1})	0.626	0.627	0.626	0.628
Refinement				
$R[F^2 > 2\sigma(F^2)]$, $wR(F^2)$, S	0.039, 0.082, 1.16	0.092, 0.186, 2.73	0.056, 0.097, 1.36	0.079, 0.164, 2.40
No. unique reflections/parameters	458 / 101	280 / 46	373 / 46	382 / 46
No. of restraints	100	25	25	25

Table S3 Absolute mean difference in the contributing energy terms between PIXEL and SAPT calculations

	ORTHORHOMBIC FORM		*MONOCLINIC FORM*	
	Absolute mean / kJ mol^{-1}		*Absolute mean / kJ mol^{-1}*	
	0 GPa	6.60 GPa	0 GPa	6.85 GPa
COMPONENT				
Coulombic	4.5	8.0	4.0	8.2
Polarisation	3.7	2.9	3.9	2.7
Dispersion	9.0	13.1	9.0	13.4
Repulsion	15.5	25.1	15.3	26.0

Table S4 Bond lengths of the two polymorphs of the amino acid L-histidine.

	Experimental structure				**DFT-Optimised structure**			
	Orthorhombic form		*Monoclinic form*		*Orthorhombic form*		*Monoclinic form*	
	0 GPa	6.60 GPa	0 GPa	6.85 GPa	0 GPa	6.60 GPa	0 GPa	6.85 GPa
Bond								
O1-C1	1.247(3)	1.247(14)	1.242(3)	1.20(3)	1.2598	1.2526	1.2590	1.2351
O2-C1	1.245(3)	1.261(7)	1.248(3)	1.236(15)	1.2674	1.2707	1.2685	1.2693
N1-C2	1.491(3)	1.479(7)	1.483(3)	1.493(17)	1.5023	1.4847	1.5025	1.4849
N2-C4	1.376(3)	1.399(7)	1.381(3)	1.402(17)	1.3982	1.3966	1.3978	1.3979
N2-C5	1.324(3)	1.309(17)	1.319(3)	1.31(4)	1.3370	1.3291	1.3367	1.3323
N3-C5	1.331(3)	1.325(12)	1.331(4)	1.31(3)	1.3611	1.3519	1.3611	1.3550
N3-C6	1.362(3)	1.370(11)	1.365(4)	1.38(3)	1.3843	1.3790	1.3842	1.3754
C1-C2	1.530(3)	1.517(17)	1.535(4)	1.51(3)	1.5448	1.5290	1.5441	1.5209
C2-C3	1.529(3)	1.523(11)	1.534(4)	1.53(2)	1.5457	1.5365	1.5456	1.5323
C3-C4	1.501(3)	1.474(15)	1.493(4)	1.47(3)	1.4996	1.4917	1.5001	1.4867
C4-C6	1.353(3)	1.343(17)	1.357(4)	1.35(3)	1.3798	1.3740	1.3806	1.3677

Table S5 Valence angles of the two polymorphs of the amino acid L-histidine

	Experimental structure				**DFT-Optimised structure**			
	Orthorhombic form		*Monoclinic form*		*Orthorhombic form*		*Monoclinic form*	
	0 GPa	6.60 GPa	0 GPa	6.85 GPa	0 GPa	6.60 GPa	0 GPa	6.85 GPa
Valence								
C4-N2-C5	104.8(2)	106.1(9)	104.9(2)	106.6(19)	105.52	106.06	105.55	105.81
C5-N3-C6	107.14(19)	106.9(10)	107.0(2)	108(2)	107.30	107.66	107.34	107.59
O1-C1-O2	126.3(2)	123.5(11)	126.3(3)	126(2)	126.57	124.24	126.42	124.18
O1-C1-C2	117.0(2)	118.7(6)	117.0(2)	116.9(13)	117.01	117.69	117.12	117.86
O2-C1-C2	116.7(2)	117.7(9)	116.6(2)	117.3(19)	116.39	118.03	116.40	117.87
N1-C2-C1	109.74(18)	107.0(9)	110.1(2)	110.2(18)	110.16	107.53	110.35	108.21
N1-C2-C3	109.9(2)	110.4(5)	110.3(2)	108.8(12)	110.30	110.13	110.57	109.85
C1-C2-C3	110.80(18)	111.3(6)	110.0(2)	111.6(13)	111.44	112.25	110.55	111.72
C2-C3-C4	112.79(18)	112.9(6)	113.5(2)	111.0(13)	112.24	112.94	112.99	110.68
N2-C4-C3	120.4(2)	120.5(9)	120.7(2)	124(2)	120.83	120.16	120.87	121.36
N2-C4-C6	109.5(2)	107.5(9)	109.2(2)	107(2)	109.26	108.68	109.27	108.86
C3-C4-C6	130.1(2)	132.0(6)	130.1(3)	128.7(13)	129.91	131.15	129.86	129.60
N2-C5-N3	112.0(2)	111.8(7)	112.3(2)	111.7(19)	111.56	111.15	111.54	111.01
N3-C6-C4	106.5(2)	107.7(6)	106.6(3)	107.4(14)	106.37	106.44	106.31	106.70

Table S6 Conformation of the two polymorphs of the amino acid L-histidine

	Experimental structure				**DFT-Optimised structure**			
	Orthorhombic form		*Monoclinic form*		*Orthorhombic form*		*Monoclinic form*	
	0 GPa	6.60 GPa	0 GPa	6.85 GPa	0 GPa	6.60 GPa	0 GPa	6.85 GPa
Conformation								
O1-C1-C2-N1	−27.3(3)	−18.4(7)	−27.9(4)	−18.0(14)	−28.99	−16.36	−29.86	−13.67
O1-C1-C2-C3	94.3(3)	101.7(7)	93.8(3)	103.0(13)	93.79	104.91	92.78	107.37
O2-C1-C2-N1	155.0(2)	164.8(5)	154.5(2)	165.9(10)	152.88	165.87	152.63	169.61
O2-C1-C2-C3	−83.4(3)	−75.1(7)	−83.7(3)	−73.1(14)	−84.35	−72.85	−84.73	−69.35
N1-C2-C3-C4	−59.0(3)	−51.0(11)	−58.0(3)	−51(2)	−56.30	−47.56	−55.21	−52.11
C1-C2-C3-C4	−180.5(2)	−168.5(6)	−179.7(2)	−172.9(12)	−178.99	−167.33	−177.72	−172.19
C2-C3-C4-N2	56.5(3)	55.1(8)	53.8(4)	56.5(17)	54.73	52.01	52.08	55.06
C2-C3-C4-C6	−123.1(3)	−125.7(8)	−127.8(3)	−114.4(15)	−124.22	−128.85	−128.87	−119.41
C3-C4-N2-C5	−179.8(2)	179.7(6)	178.8(3)	−173.4(17)	−179.04	−179.92	179.27	−173.86
C6-C4-N2-C5	−0.2(3)	0.3(7)	0.0(3)	−0.9(14)	0.12	0.77	0.04	1.64
N2-C4-C6-N3	0.4(3)	−0.4(7)	0.3(3)	1.5(13)	0.20	−0.49	0.19	−0.98
C3-C4-C6-N3	−180.0(2)	−179.7(6)	−178.3(3)	173.7(17)	−179.25	−179.70	−178.95	174.03
N3-C5-N2-C4	−0.2(3)	0.0(7)	−0.3(3)	−0.2(15)	−0.40	−0.77	−0.26	−1.70
N2-C5-N3-C6	0.4(3)	−0.2(7)	0.5(3)	1.2(15)	0.54	0.48	0.39	1.13
C4-C6-N3-C5	−0.5(3)	0.4(7)	−0.5(3)	−1.7(14)	−0.43	0.03	−0.34	−0.05

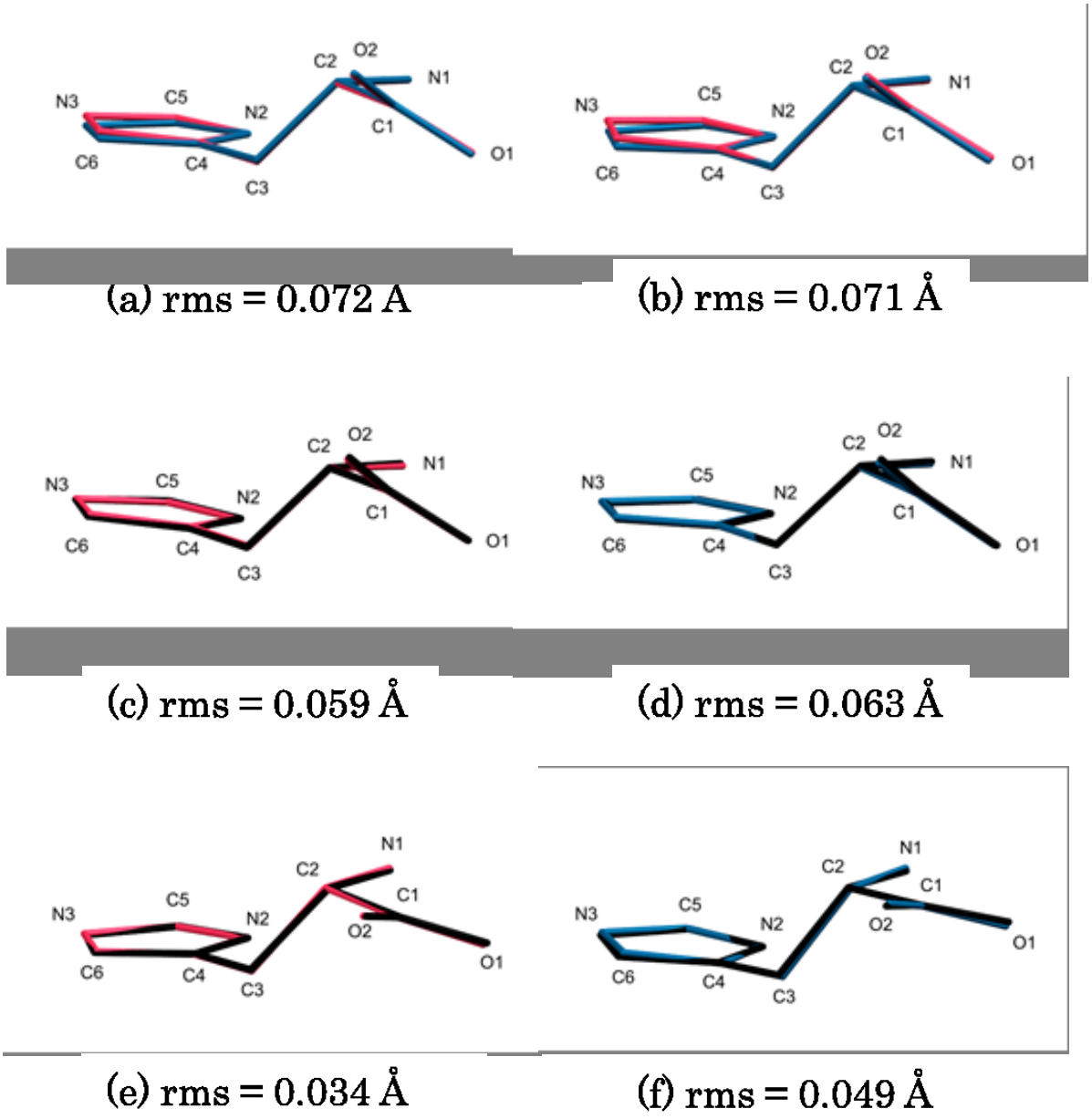

Figure S1. Comparison between the experimental (**a**) and optimised (**b**) molecular structures of the orthorhombic (pink) and monoclinic (blue) polymorphs of the amino acid L-histidine at ambient conditions. Comparison between the experimental (coloured) and optimised (black) molecular structures in the ambient-pressure phases I (**c**) and II (**d**), in phase I' (**e**) at 6.60 GPa and in phase II' (**f**) at 6.85 GPa. Hydrogen atoms are excluded from the analysis. Overlay of the structures was determined using the structure overlay feature in MERCURY.

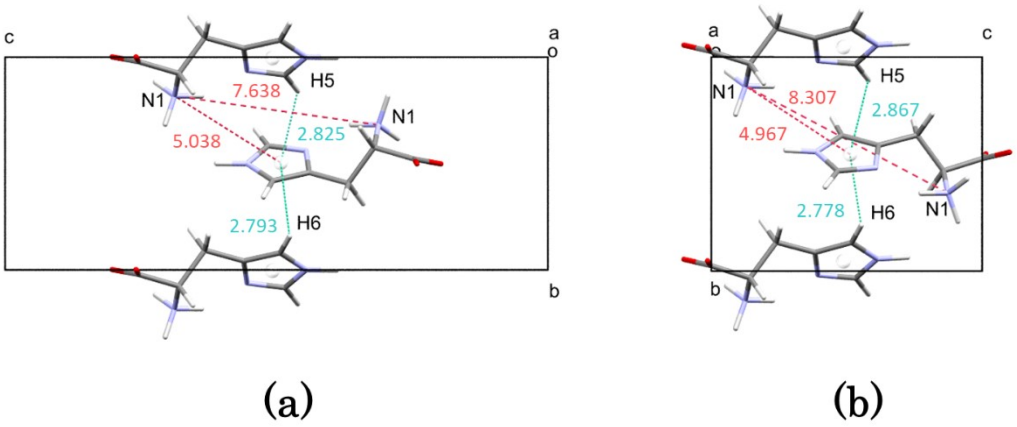

Figure S2. Stabilising intermolecular interaction between imidazole rings (green) and destabilising interaction generated by the ammonium groups (red), in the crystal structure of the orthorhombic (**a**) and monoclinic (**b**) polymorphs of the amino acid L-histidine viewed along *a* (distances between contacting groups are reported in Å)

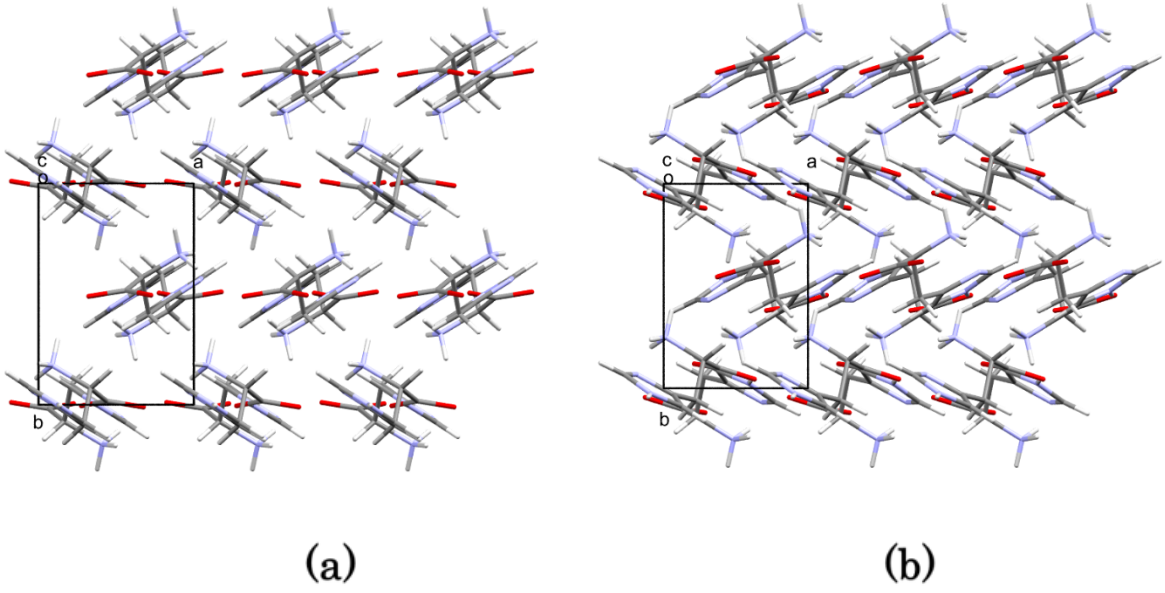

Figure S3. Crystal packing of the orthorhombic polymorphs (phases I and I') of the aminoacid *L*-histidine at ambient pressure (a) and 6.6 GPa (b), as viewed along **c**. These figures complete the description provided in Figure 3. Giving a complete view of the unit-cell content. Intermolecular interactions are omitted for the sake of clarity.

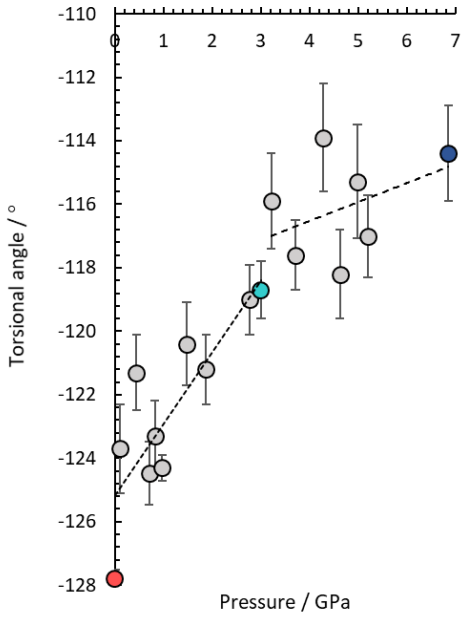

Figure S4. The torsion angle τ3 as a function of pressure, for the monoclinic polymorph of the amino acid L-histidine. The colour code is the same used in Figure 6 in the main text. Dashed trend lines were obtained through χ^2 minimisation.

Note on the variation of intramolecular bond distances with pressure

High-pressure data-sets suffer from low completeness because of shading by the diamond anvil cell, leading to low data-to-parameter ratios during refinement. It is common practice (in our group at least) in high-pressure structure analysis to restrain intramolecular bond distances and angles to those observed at ambient pressure as a means of stabilising refinements and ensuring a chemically reasonable structural model. The following note, promted by a question asked by a Referee to this paper, provides some justification for the practice.

The largest shortening in optimised bond distances in Table S4 is 0.018 Å for N1-C2 in phases I and I'. The corresponding values in phases II and II' is 0.0176 Å, also for N1-C2. These differences are beyond the precision of the measurements in the present paper.

Amongst the most precisely determined high-pressure crystal structures of organic materials has been presented by Casati *et al.*[55] and co-workers in their charge denisty analysis of an annulene derivative which 'de-aromatises' at high pressure. The differences between the bond distances measured in a 'standard' structure determination at ambient pressure (CSD Refcode BCBANN07) and a charge

density analysis at 7.7 GPa (BCBANN12, also room temperature) are listed in Table S7. The largest difference is 0.024(2) Å for C12-C13, which is similar to the value given above for histidine. In terms of Δ/σ the differences are all statistically significant. Note, however, remark made by the authors that distances from multipolar refinement on high resolution data and those from 'standard' refinements are not directly comparable because the thermal motion is better de-convoluted, giving in general slightly longer C-C distances for all bonds. Nevertheless, contractions of the order 0.02 Å might be expected below ~10 GPa.

It is not uncommon in refinements on high-pressure crystal structures to for bond distance standard uncertainties to be 0.01 Å or more. Hence, while intramolecular distances in organic compounds are affected by pressures below 10 GPa, the differences are often within the precision of the measurements unless special steps are taken to improve completeness (or if symmetry is high). For this reason application of restraints does not much affect data-fitting statistics, while at the same time improving the effective data-to-parameter ratio and thereby stabilising structure refinements.

Table S7: Comparison of bond distances at ambient conditions and 7.7 GPa for syn-1,6:8,13-Biscarbonyl[14]annulene, as reported by Casati et al. Taken from data deposited at the Cambridge Database with refcodes BCBANN07 and BCBANN12.

Bond		***d*/Å 0 GPa**	**σ(*d*)/Å 0 GPa**	***d*/Å 7.7GPa**	**σ(*d*)/Å 7.7 GPa**	**Δ/Å**	**σ(Δ)/Å**	**Δ/σ**
C1	C14	1.3941	0.0014	1.377	0.002	0.0171	0.0024	7.00
C1	C15	1.4838	0.0013	1.477	0.002	0.0068	0.0024	2.85
C1	C2	1.4071	0.0015	1.4126	0.0019	0.0055	0.0024	2.27
C10	C11	1.408	0.002	1.404	0.002	0.004	0.0028	1.41
C11	C12	1.3791	0.0018	1.395	0.002	0.0159	0.0027	5.91
C12	C13	1.4113	0.0014	1.387	0.002	0.0243	0.0024	9.95
C13	C14	1.3928	0.0014	1.405	0.0018	0.0122	0.0023	5.35
C13	C16	1.485	0.0013	1.472	0.002	0.013	0.0024	5.45
C15	O1	1.2073	0.0011	1.215	0.002	0.0077	0.0023	3.37
C16	O2	1.2087	0.0011	1.215	0.002	0.0063	0.0023	2.76
C2	C3	1.384	0.0017	1.374	0.003	0.01	0.0034	2.90
C3	C4	1.4117	0.0018	1.429	0.003	0.0173	0.0035	4.94
C4	C5	1.379	0.0017	1.373	0.002	0.006	0.0026	2.29
C5	C6	1.4117	0.0014	1.414	0.002	0.0023	0.0024	0.94
C6	C15	1.4851	0.0013	1.47	0.003	0.0151	0.0033	4.62
C6	C7	1.3953	0.0014	1.376	0.002	0.0193	0.0024	7.91
C7	C8	1.3938	0.0014	1.394	0.002	0.0002	0.0024	0.08
C8	C16	1.4851	0.0013	1.473	0.003	0.0121	0.0033	3.70
C8	C9	1.4111	0.0015	1.395	0.002	0.0161	0.0025	6.44
C9	C10	1.3784	0.0018	1.396	0.003	0.0176	0.0035	5.03

Derivation of the Relationship between Overall and Component Volumes and Bulk Moduli (Relating to Section 3.5 of the Main Text).

The isothermal compressibility κ is defined as

$$\kappa = -\frac{1}{V}\left(\frac{\partial V}{\partial P}\right)_T \qquad [1]$$

which is the inverse of the isothermal bulk modulus K

$$K = -V\left(\frac{\partial P}{\partial V}\right)_T, \qquad [2]$$

where P = pressure and V is the volume of the unit cell. The volume of the network of contacts in the unit cell (V_{net}) can be obtained as described in Section 2.6 of the main text; the void volume $V_{void} = V - V_{net}$.

The compressibility of the network can be defined as

$$\kappa_{net} = -\frac{1}{V_{net}}\left(\frac{\partial V_{net}}{\partial P}\right)_T \qquad [3]$$

with a similar relationship being defined for the voids.

Since $V = V_{net} + V_{void}$, $dV = dV_{net} + dV_{void}$, giving

$$\kappa = \frac{1}{V}\left(-\frac{\partial V_{net}}{\partial P} - \frac{\partial V_{void}}{\partial P}\right)_T \qquad [4]$$

Substituting [3] into [4] yields

$$\kappa V = \kappa_{net} V_{net} + \kappa_{void} V_{void}. \qquad [5]$$

In terms of bulk moduli ($K_{net} = 1/\kappa_{net}$ *etc*.) equation [5] is

$$\frac{V}{K} = \frac{V_{net}}{K_{net}} + \frac{V_{void}}{K_{void}} \qquad [6]$$

Note that this relationship only applies when the total volume is the sum of the component volumes.

Table S8. Parameters for the Birch-Murnaghan equations of state (EoS) of the molecule, network and void in phase I and II, at 298 K (Relating to Section 3.5 of the Main Text).

Molecular Volume		
2nd order Birch-Murnaghan EoS	**Phase I**	**Phase II**
T_0/K	298	298
$V_0/\text{Å}^3$	141.538	141.558
K_0/GPa	642(12)	513(20)
K'	4	4
K''/GPa^{-1}	–0.00605	–0.00757
$Reduced-\chi^2$	0.94	0.96
Network Volume		
2nd order Birch-Murnaghan EoS	**Phase I**	**Phase II**
T_0/K	298	298
$V_0/\text{Å}^3$	115.522	112.438
K_0/GPa	99(9)	67(2)
K'	4	4
K''/GPa^{-1}	–0.03931	–0.05832
$Reduced-\chi^2$	8.93	7.34
Void Space Volume		
3rd order Birch-Murnaghan EoS	**Phase I**	**Phase II**
T_0/K	298	298
$V_0/\text{Å}^3$	62.194	66.613
K_0/GPa	5.3(3)	4.29(15)
K'	2.46(11)	2.98(14)
K''/GPa^{-1}	–0.88678	–0.91158
$Reduced-\chi^2$	6.41	0.58

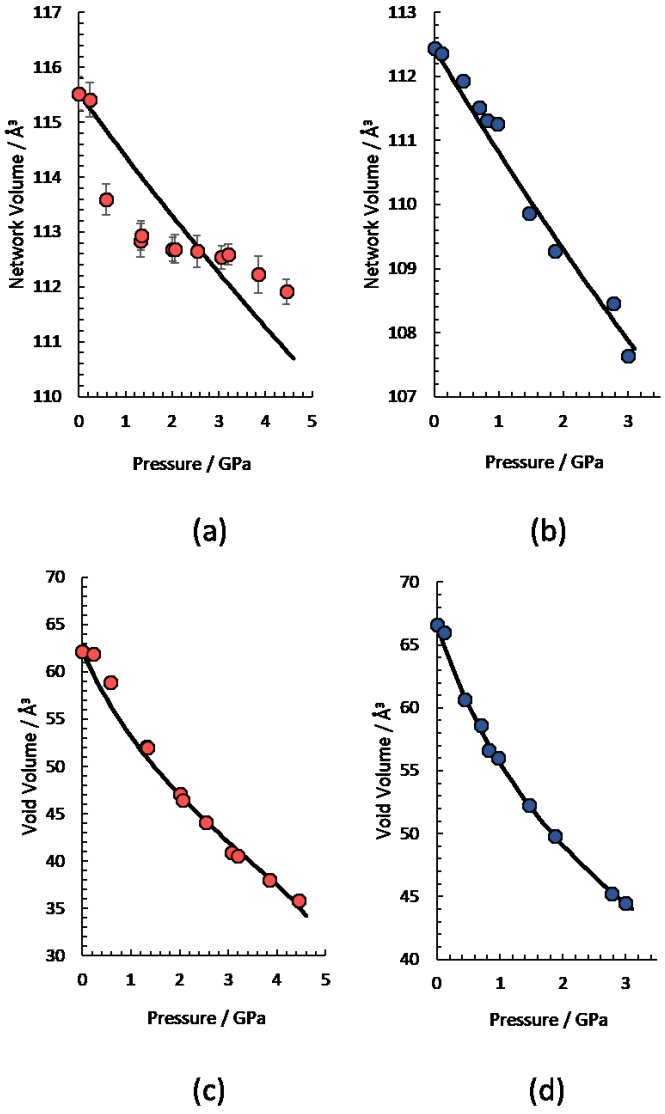

Figure S5. Black lines represent the equations of state, whose parameters are listed in the table above, of the network (**a, b**) and void space (**c, d**) for phase I (red) and II (blue) of L-histidine. Where not visible, errors are smaller than the circles. Note that fitting has been unsuccessful in the case of the network in phase I shown in part (**a**).

References

(1) Athimoolam, S.; Natarajan, S. 4-Carboxy-anilinium (2R,3R)-tartrate and a redetermination of the α-polymorph of 4-amino-benzoic acid. *Acta Crystallogr. Sect. C Cryst. Struct. Commun.* **2007**, *63*, 514–517.

(2) Ward, M. R.; Younis, S.; Cruz-Cabeza, A. J.; Bull, C. L.; Funnell, N. P.; Oswald, I. D. H. Discovery and recovery of delta p-aminobenzoic acid. *CrystEngComm* **2019**, *21*, 2058–2066.

(3) Cruz-Cabeza, A. J.; Davey, R. J.; Oswald, I. D. H.; Ward, M. R.; Sugden, I. J. Polymorphism in p-

aminobenzoic acid. *CrystEngComm* **2019**, *21*, 2034–2042.

(4) Yan, T.; Wang, K.; Duan, D.; Tan, X.; Liu, B.; Zou, B. P-Aminobenzoic acid polymorphs under high pressures. *RSC Adv.* **2014**, *4*, 15534-15541.

(5) Gracin, S.; Fischer, A. Redetermination of the β-polymorph of p-aminobenzoic acid. *Acta Crystallogr. Sect. E: Struct. Reports Online.* **2005**, *61*, 1242-1244.

(6) Benali-Cherif, R.; Takouachet, R.; Bendeif, E. E.; Benali-Cherif, N. The structural properties of a noncentrosymmetric polymorph of 4-aminobenzoic acid. *Acta Crystallogr. Sect. C Struct. Chem.* **2014**, *70*, 323-325.

(7) Drebushchak, T. N.; Chesalov, Y. A.; Boldyreva, E. V. A conformational polymorphic transition in the high-temperature ε-form of chlorpropamide on cooling: A new ε′-form. *Acta Crystallogr. Sect. B Struct. Sci.* **2009**, *65*, 770-781.

(8) Seryotkin, Y. V.; Drebushchak, T. N.; Boldyreva, E. V. A high-pressure polymorph of chlorpropamide formed on hydrostatic compression of the α-form in saturated ethanol solution. *Acta Crystallogr. Sect. B Struct. Sci. Cryst. Eng. Mater.* **2013**, *69*, 77-85.

(9) Boldyreva, E. V.; Dmitriev, V.; Hancock, B. C. Effect of pressure up to 5.5 GPa on dry powder samples of chlorpropamide form-A. *Int. J. Pharm.* **2006**, *327*, 51-57.

(10) Drebushchak, T. N.; Chukanov, N. V.; Boldyreva, E. V. A new polymorph of chlorpropamide: 4-chloro-N-(propylaminocarbonyl) benzenesulfonamide. *Acta Crystallogr. Sect. E: Struct. Reports Online.* **2006**, *62*, 4393-4395.

(11) Zakharov, B. A.; Goryainov, S. V.; Boldyreva, E. V. Unusual seeding effect in the liquid-assisted high-pressure polymorphism of chlorpropamide. *CrystEngComm* **2016**, *18*, 5423-5428.

(12) Zakharov, B. A.; Seryotkin, Y. V.; Tumanov, N. A.; Paliwoda, D.; Hanfland, M.; Kurnosov, A. V.; Boldyreva, E. V. The role of fluids in high-pressure polymorphism of drugs: Different behaviour of β-chlorpropamide in different inert gas and liquid media. *RSC Adv.* **2016**, *6*, 92629-92637.

(13) Bouvart, N.; Palix, R. M.; Arkhipov, S. G.; Tumanov, I. A.; Michalchuk, A. A. L.; Boldyreva, E. V. Polymorphism of chlorpropamide on liquid-assisted mechanical treatment: Choice of liquid and type of mechanical treatment matter. *CrystEngComm* **2018**, *20*, 1797-1803.

(14) Drebushchak, T. N.; Chukanov, N. V.; Boldyreva, E. V. Two polymorphs of chlorpropamide: The δ-form and the high-temperature ε-form. *Acta Crystallogr. Sect. C Cryst. Struct. Commun.* **2008**, *64*, 623-625.

(15) Louër, D.; Louër, M.; Dzyabchenko, V. A.; Agafonov, V.; Ceolin, R. Structure of a metastable phase of piracetami from X-ray powder diffraction using the atom–atom potential method. *Acta Crystallogr. Sect. B* **1995**, *51*, 182-187.

(16) Kanunnikova, O. M.; Mikhailova, S. S.; Karban', O. V.; Mukhgalin, V. V.; Aksenova, V. V.; Sen'kovskii, B. V.; Pechina, E. A.; Lad'yanov, V. I. Effect of deformation on the structural state of piracetam. *Russ. Metall.* **2016**, *4*, 354-360.

(17) Admiraal, G.; Eikelenboom, J. C.; Vos, A. Structures of the triclinic and monoclinic modifications of (2-oxo-1-pyrrolidinyl)acetamide. *Acta Crystallogr. Sect. B Struct. Crystallogr. Cryst. Chem.* **1982**, *38*, 2600-2605.

(18) Fabbiani, F. P. A.; Allan, D. R.; David, W. I. F.; Davidson, A. J.; Lennie, A. R.; Parsons, S.; Pulham, C. R.; Warren, J. E. High-pressure studies of pharmaceuticals: An exploration of the behavior of piracetam. *Cryst. Growth Des.* **2007**, *7*, 1115-1124.

(19) Tilborg, A.; Jacquemin, D.; Norberg, B.; Perpète, E.; Michaux, C.; Wouters, J. Structural study of piracetam polymorphs and cocrystals: Crystallography redetermination and quantum mechanics calculations. *Acta Crystallogr. Sect. B Struct. Crystallogr. Cryst. Chem.* **2011**, *67*, 499-507.

(20) Fabbiani, F. P. A.; Allan, D. R.; Parsons, S.; Pulham, C. R. An exploration of the polymorphism of piracetam using high pressure. *CrystEngComm* **2005**, *7*, 179-186.

(21) Boldyreva, E. V.; Arkhipov, S. G.; Drebushchak, T. N.; Drebushchak, V. A.; Losev, E. A.; Matvienko, A. A.; Minkov, V. S.; Rychkov, D. A.; Seryotkin, Y. V.; Stare, J.; Zakharov, B. A. Isoenergetic Polymorphism: The Puzzle of Tolazamide as a Case Study. *Chem. - A Eur. J.* **2015**, *21*, 15395-15404.

(22) Fedorov, A. Y.; Rychkov, D. A.; Losev, E. A.; Zakharov, B. A.; Stare, J.; Boldyreva, E. V. Effect of pressure on two polymorphs of tolazamide: Why no interconversion? *CrystEngComm* **2017**, *19*, 2243-2252.

(23) Fedorov, A. Y.; Rychkov, D. A.; Losev, E. A.; Drebushchak, T. N.; Boldyreva, E. V. Completing the picture of tolazamide polymorphism under extreme conditions: A low-temperature study. *Acta Crystallogr. Sect. C Struct. Chem.* **2019**, *75*, 598-608.

(24) Langan, P.; Mason, S. A.; Myles, D.; Schoenborn, B. P. Structural characterization of crystals of α-glycine during anomalous electrical behaviour. *Acta Crystallogr. Sect. B Struct. Sci.* **2002**, *58*, 728-733.

(25) Dawson, A.; Allan, D. R.; Belmonte, S. A.; Clark, S. J.; David, W. I. F.; McGregor, P. A.; Parsons, S.; Pulham, C. R.; Sawyer, L. Effect of high pressure on the crystal structures of polymorphs of glycine. *Cryst. Growth Des.* **2005**, *5*, 1415-1427.

(26) Shinozaki, A.; Komatsu, K.; Kagi, H.; Fujimoto, C.; Machida, S.; Sano-Furukawa, A.; Hattori, T. Behavior of intermolecular interactions in α -glycine under high pressure. *J. Chem. Phys.* **2018**, *148,* 044507-1/8.

(27) Hinton, J. K.; Clarke, S. M.; Steele, B. A.; Kuo, I. F. W.; Greenberg, E.; Prakapenka, V. B.; Kunz, M.; Kroonblawd, M. P.; Stavrou, E. Effects of pressure on the structure and lattice dynamics of α-glycine: A combined experimental and theoretical study. *CrystEngComm* **2019**, *21*, 4457-4464.

(28) Tumanov, N. A.; Boldyreva, E. V.; Ahsbahs, H. Structure solution and refinement from powder or single-crystal diffraction data? Pros and cons: An example of the high-pressure β'-polymorph of glycine. *Powder Diffr.* **2008**, *23*, 307-316.

(29) Shimon, L. J. W.; Lahav, M.; Leiserowitz, L. Stereoselective etchants for molecular crystals. Resolution of enantiomorphs and assignment of absolute structure of chiral molecules and polar crystals. *New J. Chem.* **1986**, *10*, 723-737.

(30) Bull, C. L.; Flowitt-Hill, G.; De Gironcoli, S.; Küçükbenli, E.; Parsons, S.; Pham, C. H.; Playford, H. Y.; Tucker, M. G. ζ-Glycine: Insight into the mechanism of a polymorphic phase transition. *IUCrJ* **2017**, *4*, 569-574.

(31) Anitha, R.; Gunasekaran, M.; Kumar, S. S.; Athimoolam, S.; Sridhar, B. Single crystal XRD, vibrational and quantum chemical calculation of pharmaceutical drug paracetamol: A new synthesis form. Spectrochim. *Acta A Mol. Biomol. Spectrosc.* **2015**, *150*, 488-498.

(32) Boldyreva, E. V; Shakhtshneider, T. P.; Ahsbahs, H.; Sowa, H.; Uchtmann, H. Effect of high pressure on the polymorphs of paracetamol. *J. Therm. Anal. Calorim.* **2002**, *68*, 437-452.

(33) Smith, S. J.; Bishop, M. M.; Montgomery, J. M.; Hamilton, T. P.; Vohra, Y. K. Polymorphism in Paracetamol: Evidence of Additional Forms IV and V at High Pressure. *J. Phys. Chem. A* **2014**, 118, 6068-6077.

(34) Ward, M. R.; Oswald, I. D. H. Antisolvent addition at extreme conditions. *CrystEngComm* **2019**, *21*, 4437-4443.

(35) Chan, E. J.; Goossens, D. J. Study of the single-crystal X-ray diffuse scattering in paracetamol polymorphs. *Acta Crystallogr. Sect. B Struct. Sci.* **2012**, *68*, 80-88.

(36) Reiss, C. A.; Van Mechelen, J. B.; Goubitz, K.; Peschar, R. Reassessment of paracetamol orthorhombic Form III and determination of a novel low-temperature monoclinic Form III-m from powder diffraction data. *Acta Crystallogr. Sect. C Struct. Chem.* **2018**, *74*, 392-399.

(37) Kolesov, B. A.; Minkov, V. S.; Boldyreva, E. V.; Drebushchak, T. N. Phase transitions in the crystals of *L*- and *DL*-cysteine on cooling: Intermolecular hydrogen bonds distortions and the side-chain motions of thiol-groups. 1. *L*-cysteine. *J. Phys. Chem. B* **2008**, *112*, 12827-12839.

(38) Moggach, S. A.; Allan, D. R.; Clark, S. J.; Gutmann, M. J.; Parsons, S.; Pulham, C. R.; Sawyer, L. High-pressure polymorphism in *L*-cysteine: The crystal structures of *L*-cysteine-III and *L*-cysteine-IV. *Acta Crystallogr. Sect. B Struct. Crystallogr. Cryst. Chem.* **2006***, 62*, 296-309

(39) Minkov, V. S.; Krylov, A. S.; Boldyreva, E. V.; Goryainov, S. V.; Bizyaev, S. N.; Vtyurin, A. N. Pressure-induced phase transitions in crystalline *L*- and *DL*-cysteine. *J. Phys. Chem. B* **2008**, *112*, 8851-8854.

(40) Minkov, V. S.; Goryainov, S. V.; Boldyreva, E. V.; Görbitz, C. H. Raman study of pressure-induced phase transitions in crystals oforthorhombic and monoclinic polymorphs of *L*-cysteine: Dynamics of the sidechain. *J. Raman Spectrosc.* **2010**, *41*, 1748-1758.

(41) Harding, M. M.; Long, H. A. The crystal and molecular structure of *L*-cysteine. *Acta Crystallogr. Sect. B Struct. Crystallogr. Cryst. Chem.* **1968**, *24*, 1096-1102.

(42) Nielsen, A. T.; Chafin, A. P.; Christian, S. L.; Moore, D. W.; Nadler, M. P.; Nissan, R. A.; Vanderah, D. J.; Gilardi, R. D.; George, C. F.; Flippen-Anderson, J. L. Synthesis of polyazapolycyclic caged polynitramines. *Tetrahedron* **1998**, *54*, 11793-11812.

(43) Millar, D. I. A.; Maynard-Casely, H. E.; Kleppe, A. K.; Marshall, W. G.; Pulham, C. R.; Cumming, A. S. Putting the squeeze on energetic materials - Structural characterisation of a high-pressure phase of CL-20. *CrystEngComm* **2010**, *12*, 2524-2527.

(44) Chukanov, N. V.; Dubikhin, V. V.; Raevskii, A. V.; Golovina, N. I.; Korsunskii, B. L.; Nedel'ko, V. V.; Aldoshin, S. M. Kinetics and mechanism of a polymorpous transition in polycrystalline epsilon-hexanitrohexaazaisowurtzitane. *Russ. J. Phys. Chem.* ***2006***, *80***,** 281-287.

(45) Ciezak, J. A.; Jenkins, T. A.; Liu, Z. Evidence for a High-Pressure Phase Transition of ε-2,4,6,8,10,12-Hexanitrohexaazaisowurtzitane (CL-20) Using Vibrational Spectroscopy. *Propellants, Explos., Pyrotech.* **2007**, *32*, 472-477.

(46) Yu, L.; Stephenson, G. A.; Mitchell, C. A.; Bunnell, C. A.; Snorek, S. V.; Bowyer, J. J.; Borchardt, T. B.; Stowell, J. G.; Byrn, S. R. Thermochemistry and conformational polymorphism of a hexamorphic crystal system. *J. Am. Chem. Soc.* **2000**, *122*, 585-591.

(47) Chen, S.; Guzei, I. A.; Yu, L. New polymorphs of ROY and new record for coexisting polymorphs of solved structures. *J. Am. Chem. Soc.* **2005**, *127*, 9881-9885.

(48) Tan, M.; Shtukenberg, A. G.; Zhu, S.; Xu, W.; Dooryhee, E.; Nichols, S. M.; Ward, M. D.; Kahr, B.; Zhu, Q. ROY revisited, again: the eighth solved structure. *Faraday Discuss.* **2018**, *211*, 477-491.

(49) Gushurst, K. S.; Nyman, J.; Boerrigter, S. X. M. The PO13 crystal structure of ROY. *CrystEngComm* **2019**, *21*, 1363-1368.

(50) Harty, E. L.; Ha, A. R.; Warren, M. R.; Thompson, A. L.; Allan, D. R.; Goodwin, A. L.; Funnell, N. P. Reversible piezochromism in a molecular wine-rack. *Chem. Commun.* **2015**, *51*, 10608-10611.

(51) Funnell, N. P.; Bull, C. L.; Ridley, C. J.; Capelli, S. Structural behaviour of OP-ROY at extreme conditions. *CrystEngComm* **2019**, *21*, 4473-4483.

(52) Chan, E. J.; Rae, A. D.; Welberry, T. R. On the polymorphism of benzocaine; A lowtemperature structural phase transition for form (II). *Acta Crystallogr. Sect. B Struct. Sci.* **2009**, *65*, 509-515.

(53) Patyk-Kaźmierczak, E.; Kaźmierczak, M. A. A new high-pressure benzocaine polymorph-towards understanding the molecular aggregation in crystals of an important active pharmaceutical ingredient (API). *Acta Crystallogr. Sect. B Struct. Sci. Cryst. Eng. Mater.* **2020**, *76*, 56-64.

(54) Chan, E. J.; Welberry, T. R. Precursor effects of the orthorhombic to monoclinic phase transition in benzocaine form (II) revealed by X-ray diffuse scattering *Acta Crystallogr. Sect. B Struct. Sci.* **2010**, *66*, 260-270.

(55) Casati, N.; Kleppe, A.; Jephcoat, A.; Macchi, P. Putting pressure on aromaticity along with in situ experimental electron density of a molecular crystal. *Nat Commun*. **2016,** *7*, 10901.